Passive 670 GHz Imaging with Uncooled Low-Noise HEMT Amplifiers coupled to Zero-bias Diodes*.

E.N. Grossman**[a], K. Leong[b], X.B. Mei[b], and W.R. Deal[b]
[a]National Institute of Standards and Technology, 325 Broadway, Boulder CO, 80304;
[b]Northrop Gruman Corporation., 1 Space Park, Redondo Beach, CA, 90278

ABSTRACT

We discuss the application of recently developed 670 GHz low-noise amplifiers based on InP HEMTs to passive indoor imaging. Packaged LNAs were integrated with commercial zero-bias diodes, and accurate measurements of system noise-equivalent temperature difference (NETD) made, using blackbody sources. The NETD values are compared with independent prior measurements (Deal et al. 2011) of LNA gain, noise figure, and bandwidth, and with cryogenic bolometer measurements made in the same test conditions. Currently, the LNA gain is not sufficient to render the ZBD noise negligible; measurements are presented that separate the two components. Low-frequency noise measurements are also presented that display the effects of 1/f noise in the ZBD and gain variations in the LNA. The implications of the low-frequency noise are discussed in terms of scanning or beam-steering strategies for an imager based on the LNAs. Raster-scanned, single-pixel images of indoor scenes are presented. They are quantitatively interpreted in terms of NETD, and angular resolution and coupling efficiency of the optics.

Keywords: Times Roman, image area, acronyms, references

1. INTRODUCTION

Active and passive imaging at millimeter-wave (mmw) and submillimeter-wave (submm) frequencies, i.e. > 100 GHz, has been of interest for over two decades [1] in terrestrial applications such as personnel screening for concealed contraband and landing aids in brownout[2]. Passive imaging, i.e. radiometry, requires considerable sensitivity, since the radiometric temperature contrasts in question are well below1K, and available integration is often below 1s, particularly if real-time video is required or scanning is employed in order to reduce pixel count. The tradeoffs between different sensor technologies with the needed sensitivity are well known: heterodyne down-conversion has high complexity and cost, due to the high frequency LO required at each signal channel, cryogenic array systems have high size, weight, and power needs due to the closed-cycle refrigerators employed, and pre-amplified direct detection has until recently been confined to W-band or lower frequency because of the lack of low-noise pre-amps.

However, major investments have been made in high frequency transistor development over the last 3-5 years [3]. These have now begun to pay off, both in terms of the frequency performance of discrete transistors, as indicated in Table 1, and in terms of useful amplifier performance (30 dB gain, 13 dB NF) at frequencies up to 670 GHz [4]. The development was undertaken with active systems (i.e. radars) in mind, and submm radars that have been demonstrated

Table I. Summary of THz transistor results obtained in the past few years.

Process	f_T(GHz)	f_{max}(GHz)	Reference
NGAS 30nm InP HEMT	600	1200	Deal 2011 [4]
TSC 130 nm InP HBT	520	1150	Urteaga 2011 [5]
TSC 250 nm InP HBT	350	600	TSCrev1 “datasheet”
IHP 130nm SiGe HBT	300	500	Rucker 2012 [6]

* This work was supported by the DARPA THz Electronics Program. The views expressed are those of the authors and do not reflect the official policy or position of the Department of Defense or the U.S. Government. Approved for public release, distribution unlimited.

**erich.grossman@nist.gov; phone 1 303 497-5102;

Passive and Active Millimeter-Wave Imaging XVII, edited by David A. Wikner,
Arttu R. Luukanen, Proc. of SPIE Vol. 9078, 907809 · © 2014 SPIE
CCC code: 0277-786X/14/$18 · doi: 10.1117/12.2050738

in the past [7] are now being adapted to incorporate the new technology. The same amplifiers can be applied to passive,

i.e. radiometric, imaging systems and that is the question addressed in the present work. We find, as detailed below, that the sensitivity of the amplifiers (1/f noise in particular) is sufficient to enable an uncooled passive system based upon them to provide the same image quality as cryogenic bolometer arrays (in indoor contraband detection applications).

Pre-amplified Direct Detection

The goal of uncooled mm-wave detectors, simple, array-compatible, and low-cost, with sufficient sensitivity for passive radiometry has been actively pursued in the past. Notably, DARPA's MIATA program[8] resulted in uncooled zero-bias diode (ZBD) arrays for the 100-200 GHz band whose noise-equivalent temperature difference (NETD) approached 2K. Though not quite sensitive enough to use alone for indoor real-time imaging, it was found that those detectors could be combined with low-noise amplifiers into a small module that provided NETD < 0.5 K [9]. A key issue for such modules is low-frequency noise, from both the zero-bias diode (which is not at exactly zero bias in operation) and the high-frequency amplifier.

The present work takes the same basic approach, combining a high-frequency, but relatively low gain, low-noise amplifier (LNA) with a sensitive zero-bias diode. We adopt the same notation and analytic framework as [9]. An important, and sometimes underappreciated, aspect of that analysis is that purely low-frequency measurements at the ZBD output are sufficient to calculate, not only the noise-equivalent temperature difference (NETD), but also the pre-amp's noise temperature and bandwidth. To obtain these three performance metrics, three low-frequency measurements are required: the DC ("self-bias") voltage on the ZBD, V, the change in this voltage with scene temperature, dV/dT_s and the white noise added to this voltage when the LNA output is applied S_V. Of course, the bandwidth and noise temperature (as well as the RF gain) may also be obtained directly from RF measurements, for example with a vector network analyzer. Some low-frequency measurements have been very briefly presented in a separate submission[10]; these are supplemented here with a comparison to separate direct VNA measurements.

2. MEASUREMENTS

2.1 Components and setup

The packaged LNA's, designed and fabricated at Northrop Gruman, are described in [4]. Two separate units were included in this study, denoted 2-1 and 2-2, the latter displaying significantly lower gain (~ 3dB) than the former. The ZBD is a commercial unit, with a measured zero-bias resistance of $R_0 = 1.75\ k\Omega$ and nominal responsivity of $\beta = 750\ \mathrm{V/W}$, (referred to the input flange). Both ZBD and LNA are packaged in WR-1.5 rectangular waveguide blocks, with standard UG-387 flanges at input and output. The ZBD responsivity was not independently measured; its frequency dependence and its deviation from the nominal value introduce some uncertainty into the comparison between low-frequency and RF data (see §3.1 below).

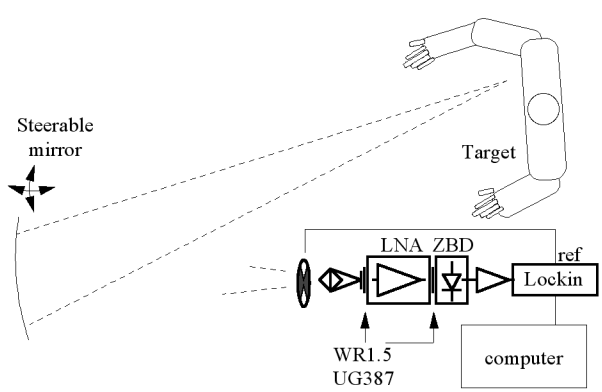

Fig. 1 Experimental configuration for imaging measurements

The low-frequency (video) output of the ZBD is fed to a low-noise (gain=100, 1.4 nV/Hz$^{1/2}$) bipolar preamp, and thence to a lockin amplifier for imaging or radiometric (thermal) responsivity measurements, or to an audio spectrum analyzer for low-frequency noise measurements. No Dicke switch is included in the LNA input, so simple optical chopping, at 50 Hz, is used to modulate the input signal and partially cancel radiometric drifts and offsets. A significant, but easily eliminated, artifact is introduced by the LNA's imperfect input match (S_{11}), when the chopper blade is aligned at particular orientations, where emission from the waveguide is coupled back into it. The antenna is a commercial, WR1.5 pyramidal horn with 3.63 x 2.77 mm entrance aperture, nominal gain of 25 dB, and 90% encircled beam radius (in the far field) of 10°.

2.2 Low-frequency measurements: "self-bias voltage" and thermal responsivity

The "self-bias" voltage in a preamplified direct-detection module is primarily caused by rectification in the ZBD of the LNA's amplified input noise, integrated over the LNA bandwidth. Using the formalism of [9] ,

$$V = \int_0^\infty G\beta S_a \, df \tag{1}$$

where G is the LNA gain and S_a the total available noise power spectral density (PSD) referred to the LNA input:

$$S_a = \alpha k\left(T_s - T_0\right) + FkT_0 \quad . \tag{2}$$

T_s and T_0 are the scene temperature and reference temperature (290 K), k Boltzmann's constant, F the LNA noise factor (i.e. noise figure in linear units), and $\alpha = \frac{|S_{21}|^2}{\left(1-|S_{22}|^2\right)}$ describes the effects of the antenna and input transition in terms of their S-parameters. The second term in (2) greatly dominates the first when viewing scenes near room temperature, although the first term is responsible for the radiometer's operation as a passive imager. The thermal responsivity, using the same definitions, is given by

$$dV/dT_s = k\int_0^\infty \alpha G\beta \quad df \quad . \tag{3}$$

This is essentially the LNA's gain-bandwidth product (adjusted for the transmittance of the antenna and transition.) The measurement results for "self-bias" voltage and thermal response of the radiometer using each of the two LNAs (separately) are shown in Fig. 2. The self-bias voltage is simply the difference in DC output of the ZBD when the LNA is turned on and off. The small offset seen when the LNA is off is real and due to rectification of the video preamp's input bias noise in the ZBD. The thermal responsivity was measured simply by placing loads of submm absorber material (Emerson-and Cuming, AN-72) cooled to liquid nitrogen (LN2) temperature in a Styrofoam container, directly in the antenna beam, immediately after the chopper. The loads were substantially oversized, to ensure the entire beam was terminated at T = 77 K. The raw lockin output is shown at the right of Fig. 2. This is converted to the module's radiometric responsivity using

$$\frac{dV}{dT} = \frac{\pi}{\sqrt{2}}\frac{V_{lockin}}{\Delta T} \quad . \tag{4}$$

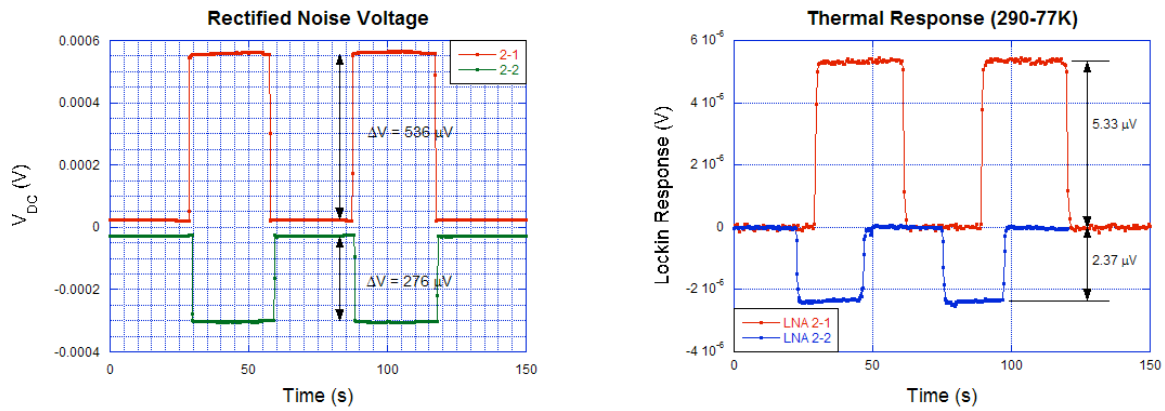

Fig.2. Self-bias voltage (left) and thermal response (right) of the radiometer, using each of the two pre-amps LNA 2-1 and 2-2 separately. The rectified noise voltage was measured at DC, the thermal response at a chopping frequency of 50 Hz. In both figures, the sign of one unit's response has been inverted for clarity.

The factor of $\pi/\sqrt{2}$ arises from standard lockin calibration; using ΔT=213K yields the responsivity values of 55.6 nV/K and 24.7 nV/K for units 2-1 and 2-2 respectively.

2.3 Imaging

Radiometric responsivities in the 20-50 nV/K range suggest that, with careful attention to low-noise techniques, high quality images can be obtained from targets with internal temperature contrasts of order 1 K, typical of indoor scenes. A substantial number of such passive images have been acquired by raster-scanning the primary mirror as shown in Fig. 1. Targets include human figures against a large plywood background and NIST's Aqueous Blackbody Calibration (ABC) source[11] against a (cluttered) laboratory background. Human figure images are shown in Fig. 3 and an ABC image in cFig. 4. In the human figure images, the lower left corner is actually a reflection in the optical table (boundary barely visible in (b) and possible (c)). The ABC source's design is optimized for 200-400 GHz. Its accuracy at 650 GHz is therefore not necessarily any better than the LN2-cooled absorber that was actually used for the calibration. The mirror is a 30 cm diameter, 1 m focal length (50 cm radius of curvature) spherical aluminum mirror. Nominal distance from horn aperture to mirror vertex was 68 cm, distance from vertex to nominal target plane, 1.2 m. Use of a spherical mirror off-axis does introduce a certain amount of astigmatism. Prior submm imaging experiments (using cryogenic bolometers) have shown this issue to be minor.

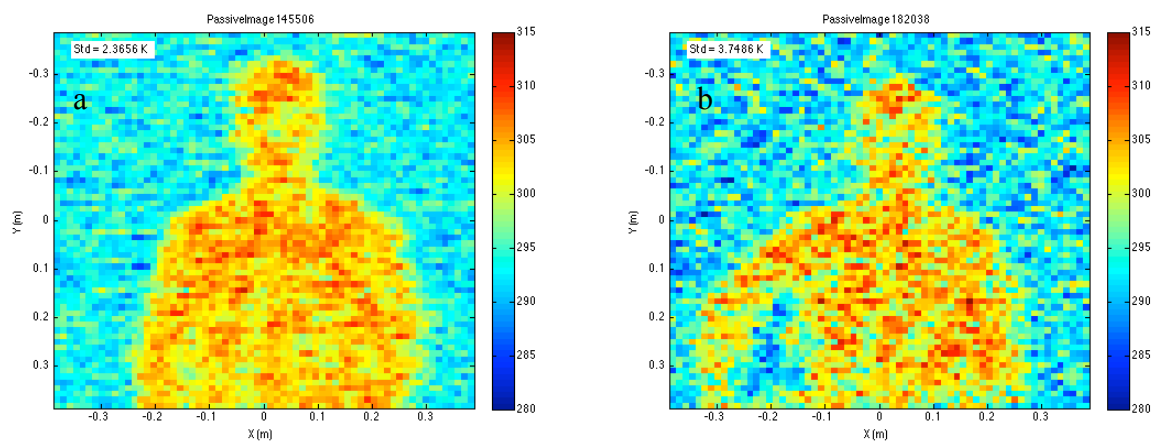

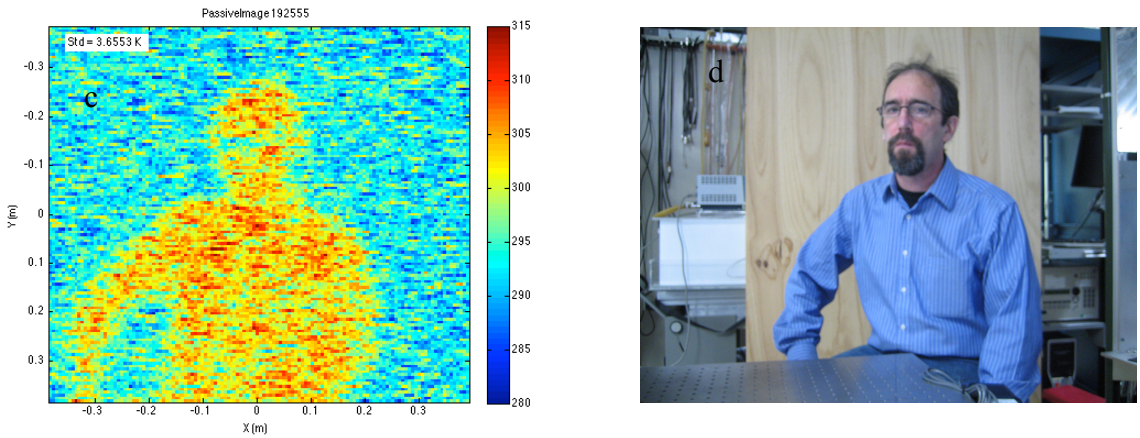

Fig. 3. Scanned single-pixel images of a human subject using the radiometer module (a,b,c), and visible image corresponding to (c). Scan parameters were 300 ms/pixel time constant, 4.2 kpixels, 22.5min total acquisition time for (a), 100 ms/pixel, 4.2 kpixels, and 14.0 min for (b), and 100 ms/pixel, 16.6 kpixel, 28.0 min for (c).

The radiometric temperature scale for all images was obtained by placing the LN2-cooled absorber in the target plane and repeating the measurement of §2.2. This indicated an aperture efficiency for the primary mirror of 65%, somewhat lower than the 90% expected from the feedhorn beam and the optical configuration. Each pixel in the 65 x 65 images shown in fig. 3a and 3b covered a 12.0 x 12.0 mm area, which represents the spatial resolution of the images. The indicated per-pixel standard deviations were evaluated simply from the upper left 19 x19 cm corner of the image. It therefore includes fluctuations unrelated to the module's noise, including real variations in background temperature, electromagnetic interference, etc. Although this clearly indicates that the module's noise performance is potentially promising for uncooled imaging of indoor scenes, a rigorous evaluation requires measurement of its noise power spectral density (PSD).

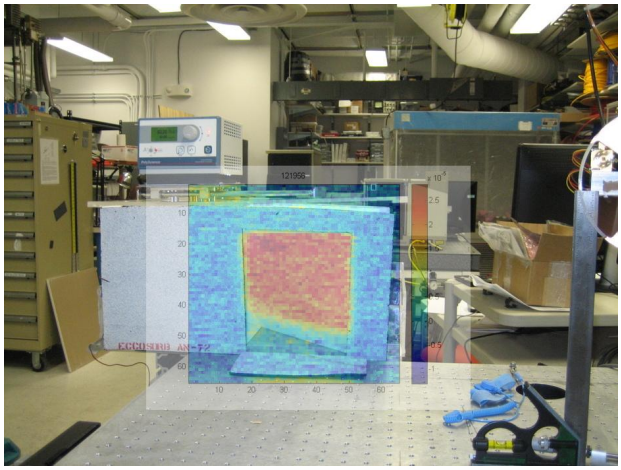

Fig. 4. Scanned single pixel image of the NIST ABC source (nominal radiometric temperature 60 C), superimposed on a visible image of the source, surrounded by its lab environment.

2.4 RF measurements

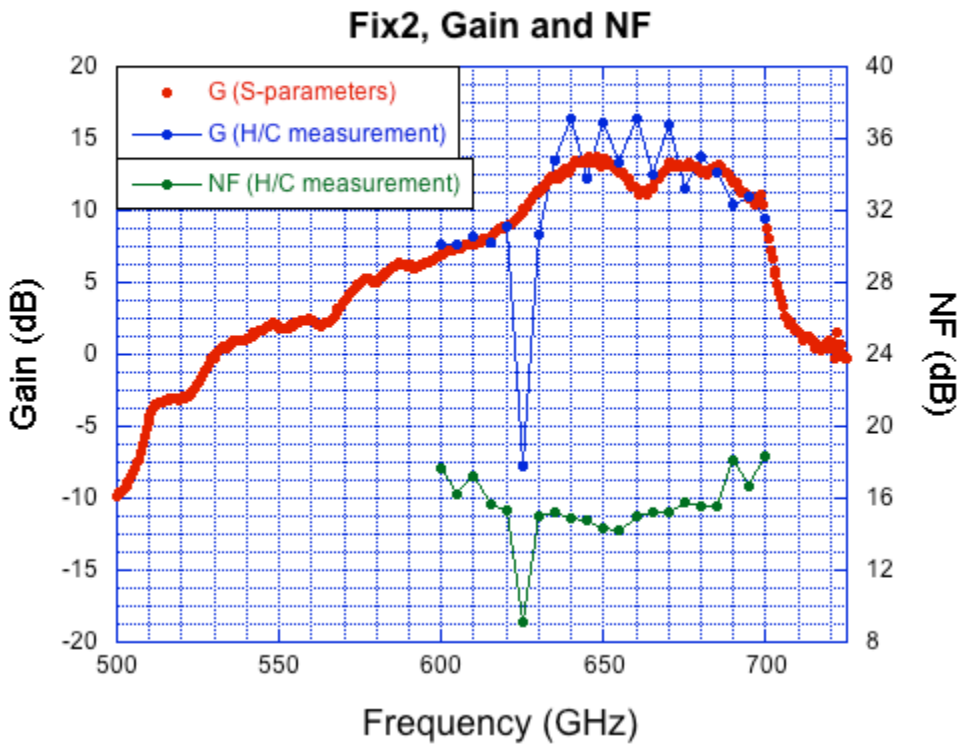

Fig. 5. RF measurements on LNA 2-2. The red points display S_{21} measured on a vector network analyzer, while the blue and green points display gain and noise figure respectively from Y-factor measurements.

Figure 5 shows frequency-dependent gain and noise figure measurements from one of the units. S-parameters where measured using a commercial vector network analyzer with waveguide extension modules. Separately, hot/cold receiver measurements were made (over 600-700 GHz) using a swept local oscillator and a low-frequency (250 MHz IF system. The latter provide both noise factor and an independent gain measurement. The two gain measurements are reasonably consistent given the completely independent calibration for the two techniques, with the notable exception of a "suckout" at 625 GHz appearing in the H/C measurements but not the S-parameters. From the irregular shape of the bandpass (not unusual for very high frequency amplifiers) it is clear that relationships between quantities like (1) and (3), that are weighted averages over frequency, may have limited accuracy (reflecting varying definitions of bandwidth).

2.5 Low-frequency noise measurements

For noise measurements, the (unchopped) feedhorn beam was terminated in room temperature absorber. The left panel of Fig. 6 displays voltage noise spectra from the module for each of the two LNA's, the spectrum produced by the ZBD alone (i.e. with LNA turned off), and the spectrum produced by the audio frequency amplifier alone (input shorted), along with fits to each spectrum. The right panel shows the same data for the two LNA's, but referred to radiometric input temperature using the thermal responsivity values mentioned above. It thus comprises the NETD spectrum.

The PSD spectra $S_V(f)$ consist of white noise S_w combined with a low-frequency component that is well-approximated by a 1/f spectrum, S_1/f. The "knee" frequency, where the two components contribute equally, lies at 500 and 100 Hz for LNA2-1, and LNA2-2 respectively. The white noise is dominated by Johnson noise of the ZBD, $\sqrt{4kT_0R_0} = 5.4\ nV/Hz^{1/2}$. However, it displays a small but significant increase, when the LNA is turned on. Referring again to [9],

$$S_V = 4kT_0R_0 + 2\int_0^\infty (G\beta S_a)^2\, df + \frac{S_1}{f} \tag{5}$$

where the first two terms $S_w = 4kT_0R_0 + 2\int_0^\infty (G\beta S_a)^2\, df$ comprise white noise, the first being Johnson noise of the ZBD and the second reflecting the LNA's input noise, which disappears when the LNA is off. Because the white noise is dominated by the ZBD, the PSD levels are nearly the same for the two units, but because of LNA 2-1's higher thermal responsivity, this level corresponds to a significantly lower white noise "floor" in NETD.

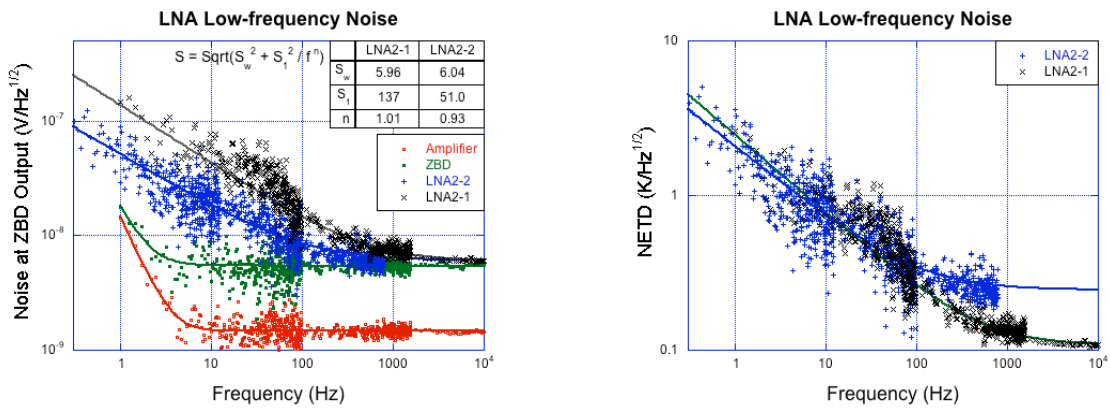

Fig. 6. Low-frequency noise spectra of the radiometer output, with LNA 2-1 or 2-2 (separately) installed. Raw voltage noise spectra are shown at (left). At (right), these same data is displayed in terms of radiometric temperature referred to the input, using the thermal responsivity shown in Fig. 2.

The low frequency component of the PSD is dominated by noise that disappears when the LNA is turned off. At 50 Hz, where the images of Figs. 3 and 4 were acquired, this component is dominant. Though superficially LNA2-1 displays significantly higher 1/f-noise than LNA2-2, this is merely a result of its higher gain, like its higher radiometric responsivity and V_{DC}. When referred to radiometric temperature at the input, the two units display the same level of 1/f-noise, within the uncertainty. The 1/f noise arises from two sources, gain fluctuations in the LNA, and 1/f noise in the (self-biased) ZBD. These cannot be separated with the present suite of measurements

3. DISCUSSION

3.1 Agreement between RF and low-frequency measurements

In Table 2 we directly compare, for the three major radiometer characteristics discussed in §1.1, the values predicted by the RF (hot/cold) measurements (eqns. (1), (3), and (5) above) and those directly measured at low frequency, on LNA2-2. Measured values for LNA2-1 are included for completeness. Agreement is reasonably good, considering the many uncertainties involved in the comparison. In all cases, the low-frequency measurements are somewhat higher than the predictions; the most straightforward explanation is that the nominal value of β that was assumed for the ZBD (750 V/W) is somewhat low. However, since V and dV/dT_s scale linearly with β while the white noise scales quadratically, the actual explanation no doubt includes more than one effect. The fact that the noise measurement first involves a fit to remove the 1/f noise, and then subtraction of the ZBD component (see eqn. (5)) makes that comparison particularly uncertain.

Table 2. Comparison of RF and low-f radiometer measurements

Quantity [unit]	Predicted from RF LNA2-1	Measured at low-f LNA2-2	Measured at low-f LNA2-1
$V\,[\mu\mathrm{V}]$	198	276	535
$(S_w - 4kT_0R_d)\left[\mathrm{nV/Hz^{1/2}}\right]$	2.03	2.80	2.41
$dV/dT_s \quad [\mathrm{nV/K}]$	19.4*	24.7	55.6

* Predicted using $\alpha = 1$ for the antenna and transition

3.2 NETD

The noise spectrum, referred to radiometric input temperature, yields the NETD spectrum. Turning this spectrum into a single number is ambiguous; the NETD displayed in an image depends on the acquisition protocol (i.e. the integration time and interval between calibrations). However, for purposes of device comparison it is common, and in the authors' opinion highly recommended, to define a "reference" NETD, corresponding to the value of the NETD spectrum at 30 Hz and an unapodized integration time of $\tau = 1/30\,\mathrm{s}$

$$NETD_{ref} = \frac{NETD\left(f = 30\mathrm{Hz}\right)}{\sqrt{2\tau}}. \tag{6}$$

This figure-of-merit comes out to 1.8K for LNA2-1 and 1.9 K LNA2-2.

With an optimal acquisition protocol, the NETD would be limited by the white noise due to the LNA's noise figure, i.e. the second term in eqn. (5). This requires sampling the noise spectrum at high enough frequency that 1/f noise is negligible and increasing the LNA gain enough that the contribution from the ZBD Johnson noise is negligible. In that case, the NETD spectral density (second row of Table 2 divided by third row) would come to 0.043 K/Hz$^{1/2}$ (for LNA2-1). Given the N$^{1/2}$ penalty in NETD paid when scanning an image, this can accommodate scanned acquisition protocols with as many as N~135 image pixels scanned (per frame) by a single radiometer channel, while still keeping the image NETD to 0.5 K or below. (This is a reasonable sensitivity threshold for attaining clutter-limited radiometric resolution in indoor environments). Useful image sizes (say 10 kpixel, see images in Fig. 3) can therefore be acquired by modest-sized (10's) arrays of radiometer channels.

REFERENCES

[1] *P. F. Goldsmith, C.-T. Hsieh, G. R. Huguenin, J. Kapitzky, and E. L. Moore, "Focal Plane Imaging Systems for Millimeter Wavelengths," IEEE Trans. Microwave The. and Tech., vol. 41, pp. 1664-1675, 1993.*

[2] *H. B. Wallace, "Analysis of RF Imaging Applications at frequencies over 100 GHz," Appl Optics, vol. 49, pp. E38-E47, 2010.*

[3] *J. D. Albrecht, M. J. Rosker, H. B. Wallace, and T.-H. Chang, "THz Electronics Projects at DARPA: Transistors, TMICs, and Amplifiers," IEEE Microwave Symposium Digest, pp. 1118-1121, 2010.*

[4] *W. R. Deal, K. Leong, V. Radisic, S. Sarkozy, B. Gorospe, J. Lee, et al., "Low Noise Amplification at 0.67 THz using 30 nm InP HEMTs," IEEE Microwave and Wireless Component Lett., vol. 21, pp. 368-370, 2011.*

[5] *M. Urteaga, R. Pierson, P. Rowell, V. Jain, E. Lobisser, and M. J. W. Rodwell, "130 nm InP DHBTs with ft>0.52 THz and fmax>1.1THz," in Device Research Conference (DRC), 2011 69th Annual, Santa Barbara, CA, 2011, pp. 281-282.*

[6] *H. Rucker, B. Heinemann, and A. Fox, "Half-Terahertz SiGe BiCMOS Technology," in 12th Topical Meeting on Si Monolithic Integrated Circuits in RF Systems (SiRF), Santa Clara, CA, 2012, pp. 133-136.*

[7] *K. B. Cooper, R. J. Dengler, N. Llombert, B. Thomas, G. Chattopadhyay, and P. H. Siegel, "Terahertz Imaging Radar for Standoff Personnel Screening," IEEE Trans. THz Sci. Tech, vol. 1, pp. 169-182, 2011.*

[8] *C. M. Stickley, Filipkowski, M., "Microantenna Arrays: Technology and Applications; MIATA an Overview," Proc. 1st Eurpoean Symposium on Optics and Photonics in Security and Defence, 2004.*

[9] *J. J. Lynch, H. P. Moyer, J. H. Schaffner, Y. Royter, M. Sokolich, B. Hughes, et al., "Passive Millimeter0wave Imaging Module with Preamplified Zero-bias Detection," IEEE Trans. Microwave Theory and Tech.. vol. 56, pp. 1592-1600, 2008.*

[10] *Grossman E.N., K. Leong, X. B. Mei, and W. R. Deal, "Low-frequency Noise and Passive Imaging with 670 Ghz HEMT Low-noise Amplifiers," Trans. THz Sci. and Tech., vol. in review, 2014.*

[11] *C. R. Dietlein, Z. Popovic, and E.N. Grossman, "Aqueous Blackbody Calibration Source for Millimeter-wave/Terahertz Metrology " Appl Optics, vol. 47, pp. 5604-5615, 2008.*